Operating force information on-line acquisition of a novel slave manipulator for vascular interventional surgery

Yan Zhao, Shuxiang Guo, Nan Xiao, Yuxin Wang, Youxiang Li & Yuhua Jiang

Biomedical Microdevices
BioMEMS and Biomedical Nanotechnology

ISSN 1387-2176
Volume 20
Number 2

Biomed Microdevices (2018) 20:1-13
DOI 10.1007/s10544-018-0275-7

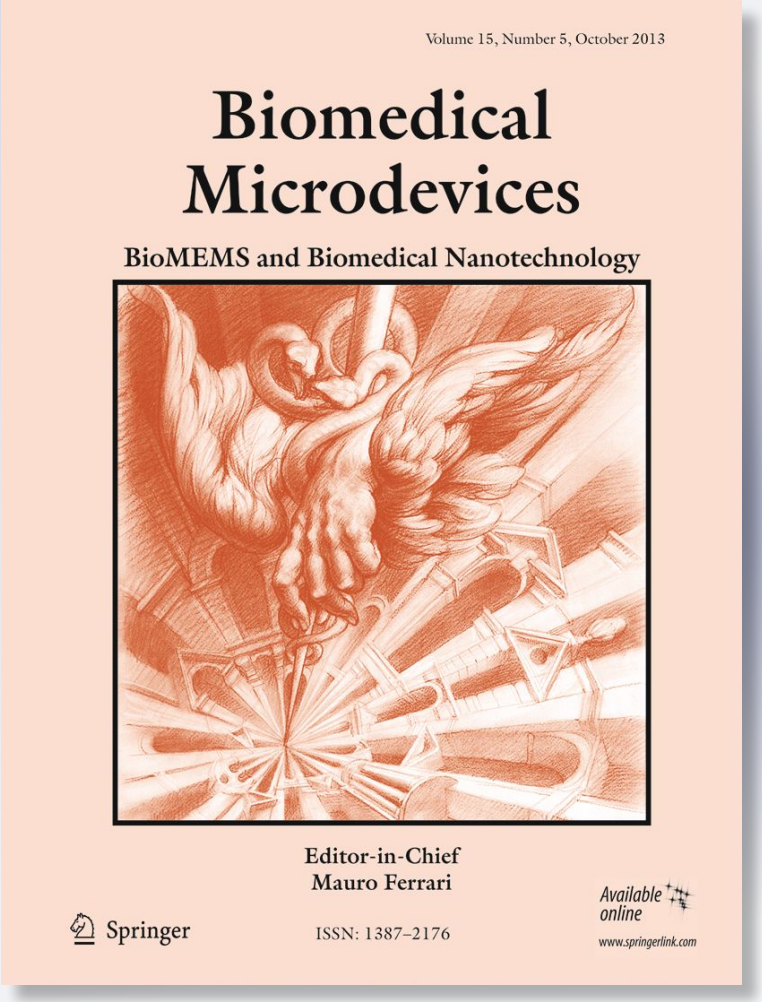

Biomedical Microdevices (2018) 20:33
https://doi.org/10.1007/s10544-018-0275-7

Operating force information on-line acquisition of a novel slave manipulator for vascular interventional surgery

Yan Zhao[1] · Shuxiang Guo[1,2] · Nan Xiao[1] · Yuxin Wang[1] · Youxiang Li[3] · Yuhua Jiang[3]

Abstract
Vascular interventional surgery has its advantages compared to traditional operation. Master-slave robotic technology can further improve the operation accuracy, efficiency and safety of this complicated and high risk surgery. However, on-line acquisition of operating force information of catheter and guidewire remains to be a significant obstacle on the path to enhancing robotic surgery safety. Thus, a novel slave manipulator is proposed in this paper to realize on-line sensing of guidewire torsional operating torque and axial operation force during robotic assisted operations. A strain sensor is specially designed to detect the small scale torsional operation torque with low rotational frequency. Additionally, the axial operating force is detected via a load cell, which is incorporated into a sliding mechanism to eliminate the influence of friction. For validation, calibration and performance evaluation experiments are conducted. The results indicate that the proposed operation torque and force detection device is effective. Thus, it can provide the foundation for enabling accurate haptic feedback to the surgeon to improve surgical safety.

Keywords Vascular interventional surgery · Robot-assisted surgery · Slave manipulator · Operating force acquisition

1 Introduction

Researches on robot-assisted vascular intervention surgery have garnered much attention in recent years. Vascular interventional surgery (Dankelman et al. 2011) has its advantages compared to traditional surgery, such as less bleeding, fewer complications, small trauma, quick recovery, etc. Robot-assisted vascular intervention surgery is considered to be a promising technology to further improve the surgical technique accuracy, efficiency and safety of vascular intervention (Vitiello et al. 2012). The research in this field is primarily focused on robotic systems and virtual-reality simulators, such as the Sensei Robotic Catheter System (Dello et al. 2016), Amigo catheter system (Datino et al. 2015), Catheter Guidance, Control, and Imaging Magnetics system (Filgueiras-Rama et al. 2013), and the Stereotaxis Niobe system (Kiemeneij et al. 2008). Thakur et al. (2009a) developed a type of remote catheter navigation system that provides users with a catheter manipulator that feels like a real catheter. Guo et al. (2012) proposed a novel in-pipe robotic control system, which implements a master-slave control mode and is remote-controlled. Wang et al. (2015, 2016) introduced a standard linear solid model to formulate a physical vascular model for application in the virtual-reality simulator of a robotic catheter system. Gelman et al. (2016) developed a catheter contact-force controller for implementation in a cardiac ablation therapy master-slave robotic system. Most of these robot-assisted vascular intervention systems implement a master-slave remote structure purposed to protect the surgeon from radiation. Furthermore, the catheter and guidewire with a large contact force that exceeds a certain safety threshold would lead to the rupture of blood vessels and consequently risk the life of the patient. Therefore, on-line acquisition of catheter and guidewire operation force information is one of the most critical safety concerns for robot-assisted surgery.

Haptic feedback via the master controller is essential for surgeons to obtain a non-visual sense of the operating

✉ Shuxiang Guo
guoshuxiang@bit.edu.cn

✉ Nan Xiao
xiaonan@bit.edu.cn

[1] Key Laboratory of Convergence Biomedical Engineering System and Healthcare Technology, The Ministry of Industry and Information Technology, School of Life Science, Beijing Institute of Technology, No.5, Zhongguancun South Street, Haidian District, Beijing 100081, China

[2] Faculty of Engineering, Kagawa University, 2217-20 Hayashi-cho, Takamatsu, Kagawa 760-8521, Japan

[3] Department of Interventional Neuroradiology, Beijing Neurosurgical Institute and Beijing Tiantan Hospital, Capital Medical University, Beijing 100050, China

Published online: 02 April 2018

conditions from the perspective of the slave manipulator, as is shown in Fig. 1. During manual surgical vascular intervention operations, the surgeon senses the contact conditions of the catheter and guidewire within the body of a patient via direct feel of the torque and force. In robot-assisted surgery, the surgeon performs the operation by the control handle of the master controller to remotely control the slave manipulator to manipulate catheter and guidewire within the body of a patient. The slave manipulator sensing system detects the torsional torque and axial force of the catheter and guidewire and then sends this information in real time to the master system. Thus, the haptic feedback is provided in real time to the surgeon via the control handle of the master controller, as is based on the force and torque signal detected by the slave manipulator. Several researchers have conducted studies in this field, including Yin et al. (2015), who integrated a human operator-centered haptic interface design concept into actuator choice and design. A semi-active haptic interface was designed and fabricated by exploiting the properties of magnetorheological (MR) fluids; subsequently, a mechanical model was established. In another similar study by Yin et al. (2014), the properties of MR fluids were again exploited to develop a haptic catheter system for teleoperation. In this latter system, the haptic sensation is provided by adjusting the magnetic field, which is dependent on the force measured in the slave manipulator, to accordingly change the viscosity of the MR fluids. Song et al. (2017) proposed an MR-fluid property-based haptic interface for endovascular tele-surgery. Guo et al. (2016) presented a force feedback unit used to provide a sense of resistance force. The force feedback in the axial direction was provided by the magnetic force generated between the permanent magnets and the powered coil. In a different study by Guo and Shuxiang (2016), a damper was developed by applying intelligent flow control of MR fluid to realize the force feedback. The damper has a piston structure with MR fluid. It should be noted that, realization of haptic feedback relies on the force information detected by slave manipulator.

To provide surgeons with haptic feedback, it's necessary to equip these surgeries with on-line detection of operating force information from catheter and guidewire controlled via the slave manipulator. However, the operating torque and force both occur on a small scale in vascular intervention surgery. In addition, guidewire and catheter are rotated at a small frequency. Research by Thakur et al. (2009b) stated that a force of 0.29 N and torque of 1.15 mN·m are required so that to move the catheter through the introducer sheath in percutaneous transluminal catheter procedures; moreover, they stated that the maximum operating torque was 15 mN·m so that to overcome vasculature friction. Thus, Xiao et al. (2012) developed a robot-assisted catheterization system. It detects the resistance force on the proximal end of the guidewire by a load cell that integrated within the slave manipulator. Additionally, Laura (Cercenelli et al. 2017) developed a remote catheter navigation system called CathROB, which detects the operating force on the catheter, and displays the force signal on the viewing monitor; consequently, the system can also signal the surgeon to discontinue force application if the force exceeds a predefined threshold. Guo et al. (2015) detected the operating force of the slave manipulator by implementing a load cell that is fixed onto the slide platform. Zhang et al. (2017) designed a strain-gauge force sensor for a haptic robot-assisted catheter

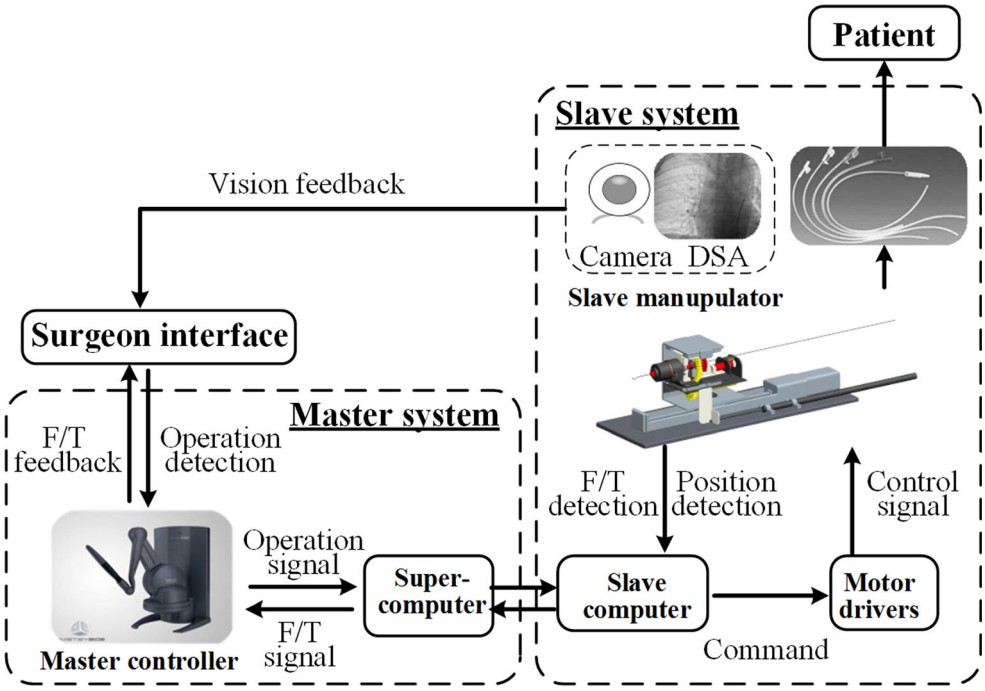

Fig. 1 Schematic diagram of the interventional assistance robotic system

operating system. Back et al. (2015) implemented a strain gauge to measure tension on a tendon-guided catheter. In this operating force detecting method, detection accuracy of operation force is deduced by friction and inertial effect of force transferring mechanism. It directly increases the difference between the feedback force to the surgeon and real operating force at slave manipulator. Moreover, operation torque with small scale and frequency is still difficult to be detected on line. Although there have been numerous studies, on-line detection of operation force and torque remains as one of the most critical concerns affecting the safety assurance of current vascular intervention robotic systems.

Thus, in this paper, a novel slave manipulator is proposed to enable on-line acquisition of operating force information of the tips of the catheter and for surgical vascular intervention. In Section 2, a novel strain-based sensing system is proposed for the detection of operating torque with small-scale and low rotational speed based on a specially designed elastic mechanism. Operating force is detected by a load cell with a designed force transferring mechanism. In Section 3, the experimental setup is developed and the calibration and evaluation experiments are explained. In Section 4, the experimental results are analyzed, and in Section 5, the research study is concluded, and future work is discussed.

2 Methods

2.1 Analysis of operation torque and force in robotic assisted vascular interventional surgery

In robot-assisted vascular intervention surgery, the freedom degrees of the slave manipulator are primarily restricted to the axial and circumferential direction for realizing axial and rotational motions of the catheter or guidewire. The structure of proposed slave manipulator is shown in Fig. 2. The axial motion is realized via a servo motor (SGMJV-01ADE6S, with the rated speed of 3000 rpm, and the rated torque of 0.318 N·m, made by Yaskawa electric corporation) and a ball screw (SKR/KR26, with the travel distance of 240 mm, made by THK). The circumferential motion is realized via a DC moter (EC-max 16, with the no-load speed of 12,000 rpm, provided with a planetary reduction gear box of GP 16C with the reduction ratio of 84:1 and a driver of ESCON 50/5, all made by Maxon) and a herringbone gear pair. The circulatory operating procedure of the proposed slave manipulator (shown in Fig. 3) is as follows:

Step 1: Drive the ball screw via the servo motor to move the sliding block of the ball screw to the starting point of its travel distance. Electrify the electromagnet (customized, with the maximum attraction force of 2.4 N, the rated voltage of 24DCV, the rated wattage of 7 W), which then pulls a block to tighten the part Q of the clamping device. Structure of the clamping device is shown in Fig. 6. Then, drive the gear pair via the DC motor to rotate the part P until the catheter or guidewire is clamped. Turn off the electromagnet to loosen part Q of the clamping device. Thus, the catheter or guidewire is clamped.

Step 2: Drive the servo motor to push or pull the catheter or guidewire. In the case of passing a vessel junction, the catheter or guidewire need to be rotated for turning into the appropriate vessel branch. Driving the herringbone gear pair via the DC motor. The clamping device is rotated together with the driven herringbone gear. Thus, the guidewire or catheter that is clamped by the clamping device could be rotated.

Step 3: When the maximum ball-screw travel distance of the manipulator is reached, electrify the electromagnet to tighten the Part Q of clamping device. Then, drive the gear pair reversely by the DC motor to loosen the catheter or guidewire. Then, drive the ball screw via the servo motor to move the salve manipulator backward to the starting point of the ball-screw.

Step 4: When the sliding block arrives at the starting point of the ball screw, clamp the catheter or guidewire again. Then, repeat these four steps until the catheter or guidewire tip reaches the focus point.

During the operation procedure, there are three kinds of force applied to the catheter and guidewire, the friction force between vessel wall and the catheter and guidewire, viscous

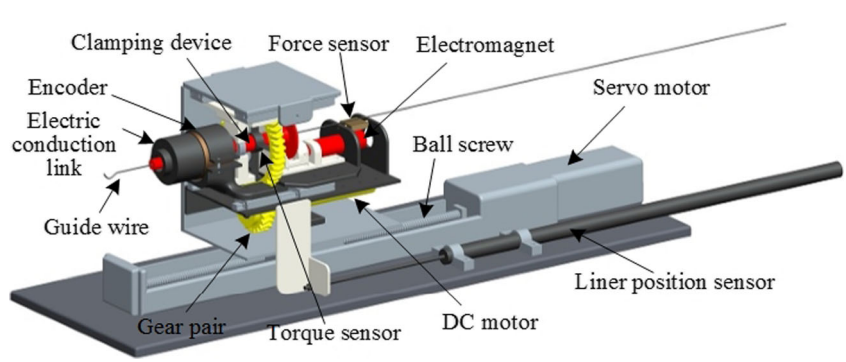

Fig. 2 The proposed slave manipulator

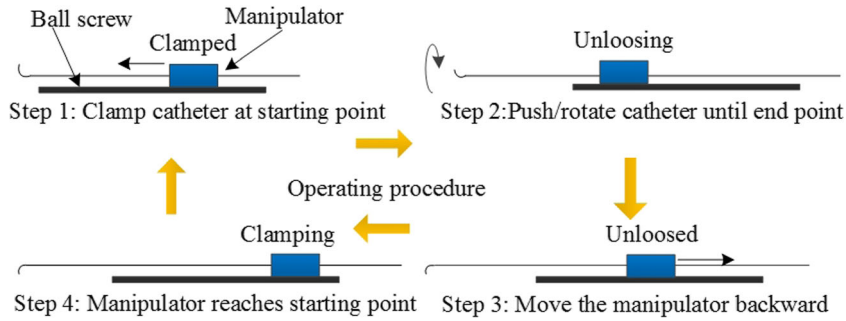

Fig. 3 Slave manipulator operating procedure

force between blood and the catheter and guidewire and impact force between vessel wall and the tips of the catheter and guidewire (as shown in Fig. 4). In addition, the sheath also applies friction force to the catheter and guide wire. The proposed sensing devices in this paper aims to realize the detection of the total consultant force at the proximal end of the catheter or guide wire, where the surgeon usually grasps during traditional surgery. The haptic feedback at master controller based on the detected total consultant force information can provide the surgeon a familiar feel similar to traditional surgery. In this way the surgeon at master side can evaluate the operation conditions at slave side during remote robot assisted surgery. The remainder of this section describes the process of on-line detection of the resultant force and torque.

2.2 Design of operation torque sensing device

As is previously stated, accurate catheter and guidewire operating torque information are necessary to ensure patient's safety during surgery; however, because the catheter and guidewire operating torque and rotational speed occur on a small scale, the conventional torque sensor cannot detect the torque. Therefore, this section describes the development of the proposed strain gauge-based operating torque sensing device that is integrated into the slave manipulator. The detected operating torque information would be send in real time to the master controller to provide haptic feedback to the surgeon.

The designed torque sensing device is shown in Fig. 5. The torque sensing device is positioned between the rotational driving herringbone gear and the guidewire clamping device. The bearings shown in Fig. 5 is made by MISUMI. The torque sensing device mainly comprises a cross beam as the elastic component, and a strain gage as the sensing element. The cross beam simultaneously acts as the elastic element of a sensing system and gear spokes. During robot assisted operations, the guidewire or catheter is clamped by using the clamping device, which is fixed with the cross beam. As is shown in Fig. 6, the operating torque τ_r is transmitted to the elastic cross beam via clamping device. It should be noted that the operating torque will lead to deformation of the crossbeam and strain gauge installed on the beam segment.

The strain gauge plays the role of a bridge beam of a Wheatstone bridge. Small strain gauge resistance changes caused by strain gauge deformation can be detected by the Wheatstone bridge. Because the torque must be detected as the clamping device and sensing device are being rotated, power line and output signal line of the Wheatstone bridge path through a cabling channel on the clamping device connected to the electric conduction link (SNH012A-08, with the electrical noise less than 10 mΩ, the inner diameter of 12.7 mm and external diameter of 35 mm, made by Senring Electronics Co. Ltd). The electric conduction link is used to link the torque sensing device with the peripheral equipment. Then, the millivolt-scale output voltage signal is amplified by an AD620 module and collected by a CONTEC DAQ card.

The accuracy and sensitivity of the sensing system are significantly affected by the elastic element. A large deformation of the elastic element under a given load yields a large strain of the strain gage, which leads to a large change of the strain gage resistance and a large output voltage of Wheatstone bridge. Hence, a larger resolution ratio of the sensing system is achieved. Moreover, although the elastic element of smaller rigidity material could provide relatively large deformation under the given load, it leads to large mechanical hysteresis, thereby reducing the response speed of the sensing system. However, the elastic element of high-rigidity material would

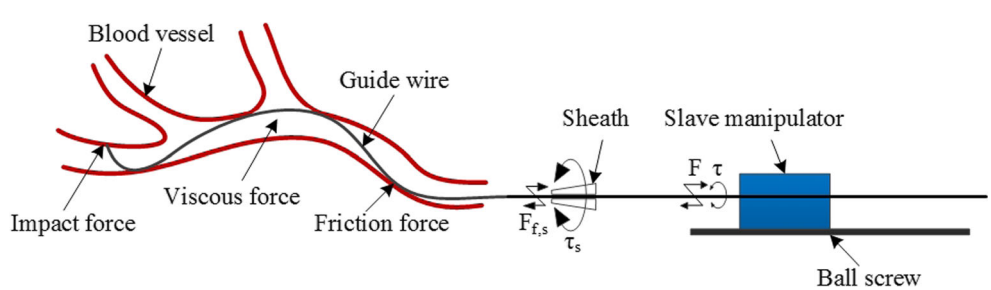

Fig. 4 Diagram of operation torque and force of guidewire

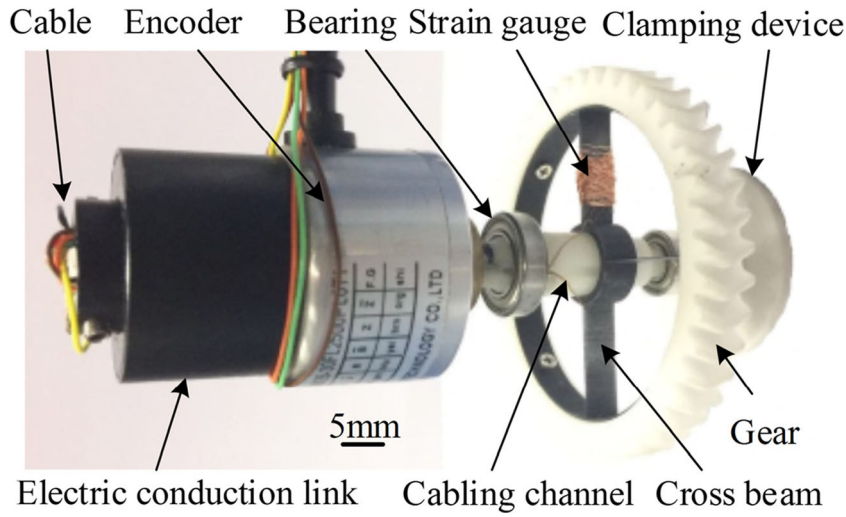

Fig. 5 Diagram of proposed torque sensing device

reduce the resolution ratio and detection accuracy. In this study, 65Mn spring steel with a high elasticity modulus of 1.98 × 105MP is employed. A single beam is designed to be with 0.2 mm thickness, 20 mm length and 7 mm width. In addition, to improve the resolution and accuracy of detection, the strain gage should be fixed at the most suitable point, which equates to the position of the largest deflection.

The stress condition of the cross beam is shown in Fig. 7. The catheter or guidewire is rotated by the driving torque of the herring gear overcoming the operation torque. It is assumed that the driving torque is equal to the operation torque, and that the stress condition of the cross beam is a static problem. Because the beam is fixed with external and internal sleeves, the stress condition could be considered as a combination of stress conditions illustrated in Fig. 8a and b. Deflections at Point x on the beam under these two stress conditions are respectively given in Eq. (1).

$$W_x = W_{x,F1} + W_{x,F2} \tag{1}$$

$$W_{x,\ F1} = \frac{F_1 x^3}{6EI_Z} \tag{2}$$

$$W_{x,F2} = \frac{1}{6EI_Z}\left[R_A\left(3l^2x - x^3\right) - 3F_2b^2x + F_2(x-a)^2\right] \tag{3}$$

$$R_A = \frac{F_2b^2}{2l^2}\left(3 - \frac{b}{l}\right) \tag{4}$$

where E is the elasticity modulus, and I_Z is the moment of inertia of a beam cross section; I_Z is given in Eq. (4).

$$I_Z = \frac{d \cdot h^3}{12} \tag{5}$$

Then, substitute Eq. (4) into Eq. (3), Eq. (5) into Eqs. (2) and (3), and Eqs. (2) and (3) into Eq. (1). Consequently, the deflection on the beam at Point x can be given as Eq. (6).

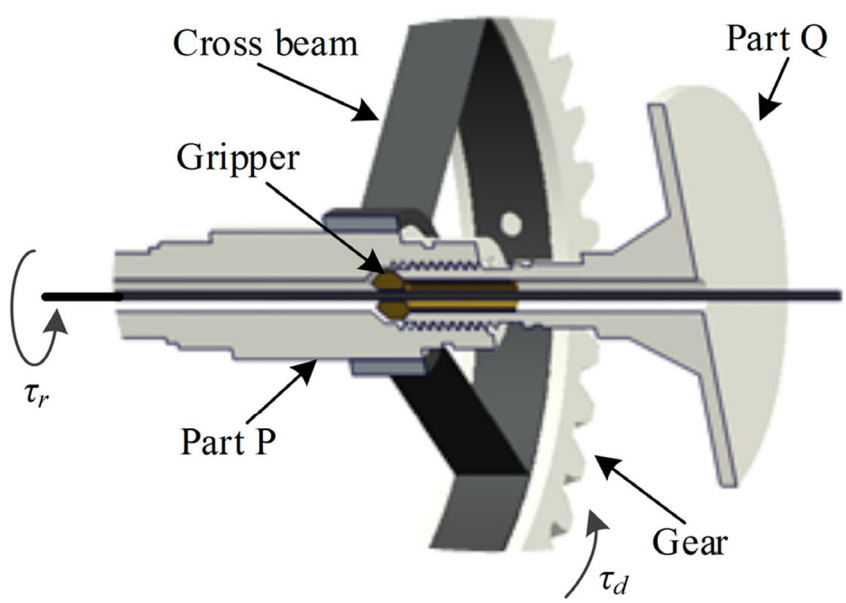

Fig. 6 Localized sectional view of the torque sensing device

$$W_x = \frac{2}{Edh^3}\left\{\left[\frac{F_1 - F_2 b^2}{2l^2\left(3-\frac{b}{l}\right)}\right]x^3 + F_2 x^2 + \left[3\frac{F_2 b^2}{2}\left(3-\frac{b}{l}\right) - 3F_2 b^2 - 2F_2 a\right]x + F_2 a^2\right\} \tag{6}$$

$$\varepsilon(x) = W^{'}(x) = \frac{2}{Edh^3}\left\{3\left(F_1 - 3\frac{F_2 b^2}{2l^2} + \frac{F_2 b^3}{2l^3}\right)x^2 + 2F_2 x + 9\frac{F_2 b^2}{2} - 3\frac{F_2 b^3}{2l} - 3F_2 b^2 - 2F_2 a\right\} \tag{7}$$

$$\varepsilon_{\max} = W'_{\max}(x) = \frac{2}{Edh^3}\left[-\frac{F_2{}^2}{3F_1 - 3\frac{F_2 b^2}{2l^2} + \frac{F_2 b^3}{2l^3}} + \frac{3}{2}b^2 - \frac{3F_2 b^3}{2l} - 2F_2 a\right] \tag{8}$$

The first derivation of Wx with respect to x can be given as Eq. (7). Deflection of the beam can be considered as the integration of deformation occurring along every segment of the beam. Thus, W′(x) represents the strain of the segment at Point x; the maximum strain of the beam segment at Point x can be expressed as Eq.(8).

Here, it is assumed that all minute elements yield the same value of strain as measured via the strain gauge, which is fixed to the beam at the location of maximum strain; thus, the measured strain is $\varepsilon_{\max}$. The relationship between the strain and change in resistance of the strain gauge can be given as Eq. (9).

$$\frac{\Delta R}{R} = K\varepsilon_{\max} \tag{9}$$

where K is the sensitivity coefficient related to strain gage material properties. As a Cu-Ni alloy strain gauge with 350 Ω resistance is adopted in this research, the corresponding K value equals 2.

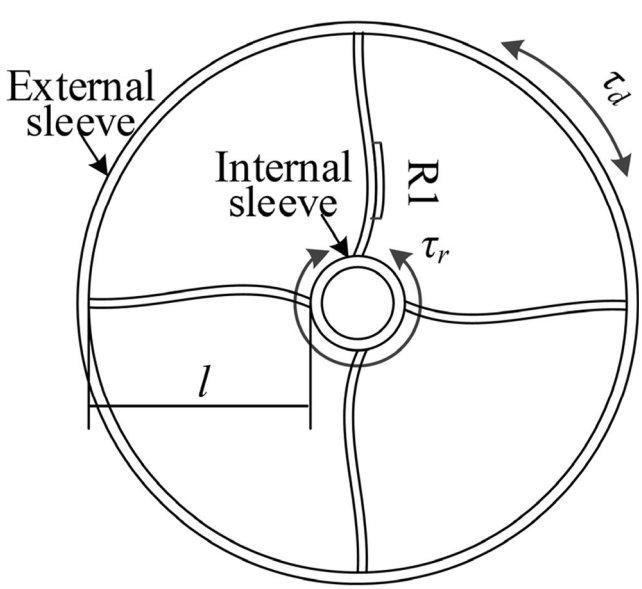

Fig. 7 Schematic diagram of the torque sensing device

As is shown in Fig. 9, R1, R2, R3, and R4 are the respective resistances of the four strain gauges fixed to the four beams. ΔR is the change in resistance of the strain gauge under the given strain. Here, it is assumed that R1 = R2 = R3 = R4 = R = 350 Ω. Then, the output voltage of the full bridge circuit can be simply expressed as Eq. (10).

$$U_{out} = \frac{\Delta R}{R}E = K\varepsilon_{\max}E \tag{10}$$

2.3 Feed-back force detection structure design

In several previous studies, the effects of mechanical friction and inertia were proved to significantly affect operating force detection. Thus, the operating force detection device is proposed in this section to diminish the effects of friction. As is shown in Fig. 2, the proposed operating force detection device mainly comprises a high-precision load cell (FSH03872, with the measuring range of 4.5 N, the nonlinearity of ±0.1% and the size of 17.5 mm × 16.5 mm × 6.7 mm, made by ADVANCED SENSOR TECHNOLOGY. INC), a guide trip slide set, a ball spline pair, and a herringbone gear pair. The guidewire clamping device is assembled with the guide trip slide set by using two bearings and a mounting plate. The driving herringbone gear is connected to the actuating shaft by a ball spline pair. Because the ball spline pair is free to move along the axial direction as it transmits the driving torque, the entire clamping device is also free to move along the axial direction. The load cell is assembled between one liner guide pair mounting plate and a fixed mounting plate. During an operation, the operating force is applied to the clamping device and then transmitted to the load cell to enable detection of the operating force.

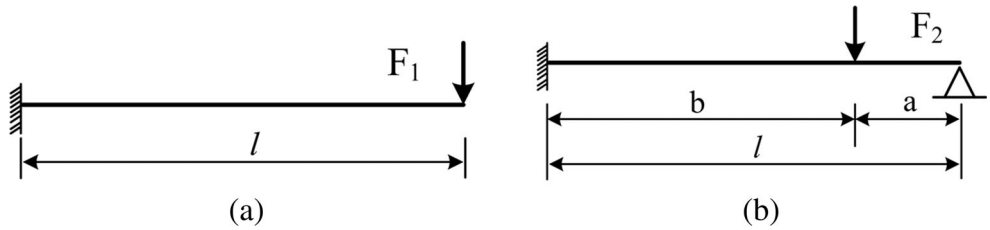

Fig. 8 Schematic diagram of equivalent loading

3 Evaluation experiments and results

The verification experiments are designed and conducted to evaluate the proposed slave manipulator from the perspective of operation torque and force acquisition performance. Medical guidewire with the diameter of 0.035in is used. According to the corresponding clinical operation specification (Liu et al. 2006), the guidewire soaks in the normal saline for 15 min prior to beginning the operation to reduce the friction coefficient of guidewire surface. However, it should be noted that, because the liquid inside the endovascular evaluator (EVE, made by FAIN-Biomedical, Inc, Japan) that is used to simulate human blood vessels in experiments is not real blood, heparinized saline is not used to soak the guidewire.

3.1 Calibration and evaluation of proposed torque sensing system

Because the sensing system transforms the crossbeam strain to a torque signal, it is important to identify the relationship between the measured torque and voltage output of the torque sensing device. However, this relationship is complex and variable because of the complex material properties, structure of the elastic component, and uncertainty of the strain gauge attachment condition. Therefore, in this section, this relationship is quantified via experimental methods.

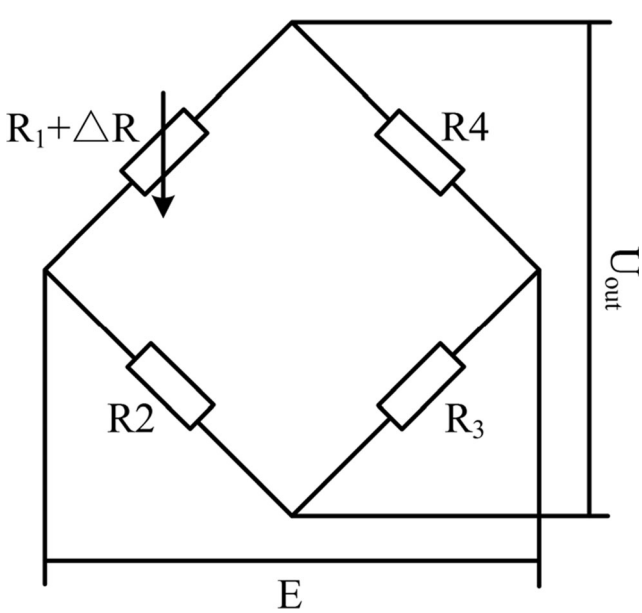

Fig. 9 Wheatstone bridge circuit diagram of the strain gages

The calibration experimental setup is shown in Fig. 10a. The entire setup, including a six-axis force/torque sensor system is fixed to an optical vibration isolation stage to eliminate noise originating from environmental vibrations. The proposed torque sensing system designed in this study is coaxially fixed to the Force/Torque transducer (Gamma SI-65-5, with the measuring range of 5000 mN·m and the accuracy of 0.75 mN·m, produced by ATI Industrial Automation, Inc, provided with a SI-65-5 ATI controller) by means of a specially designed fixture. In the torque calibration experiments, the gear of the sensing system is rotated both clockwise and anticlockwise with reciprocating torque of gradually increasing peak values. Each test is repeated ten times. The recorded values include the torque value obtained via the ATI sensor, and voltage output value obtained via the torque sensing device.

The peak values of the detected data are implemented in regression analysis by using the least-squares fitting method to quantify the relationship between the torque and digital voltage signal as obtained via implementation of the proposed operating torque sensing device. The fitted equation is shown in Fig. 11 with a linear dependence of 0.9958.

Figure 12 depicts the results of the torque signal error analysis, as detected by the proposed torque sensing device, and as compared to the torque signal detected by the ATI sensor. The torque applied to the operating torque sensing device ranges from −62 to 39 mN·m. The maximum torque detection error is 7.9894 mN·m; the maximum relative torque detection error is 7.91%. The average torque detection error is 0.2397 mN·m. The average relative error is 0.24%, with a standard deviation of 2.7633 mN·m. The mean relative errors of torque detection for ten calibration experimental trials are shown in Fig. 13. It can be seen that the maximum and minimum mean relative errors are 1.45% and 0.17%, respectively. The standard deviation is 0.31%.

The calibration experiments are conducted under conditions of steadily varying torque, while the change in operating torque is irregular during actual vascular intervention surgery. Because of this non-equivalence, performance evaluation experiments are conducted by using the experimental setup shown in Fig. 10b. The robotic system is fixed onto a platform. A specially designed fixture is used to clamp the ATI

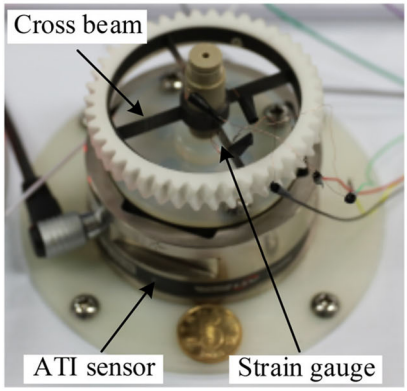

(a)

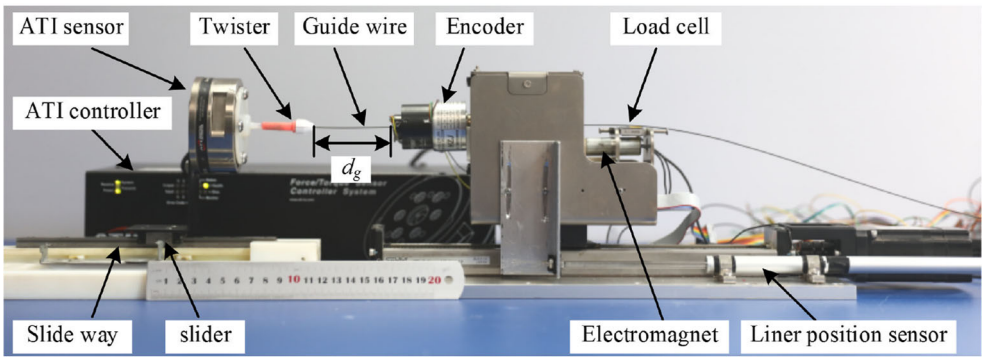

(b)

Fig. 10 Experimental setup for: (**a**) torque sensing system calibration, and (**b**) force and torque detection evaluation

sensor on a slide way, which is coaxial with the clamping device that is installed within the slave manipulator. A medical guidewire twister is coaxially fixed onto the ATI sensor. The force and torque detected by the ATI sensor is adopted as the standard for evaluation of the clamping device. Furthermore, to simulate actual vascular intervention surgery, irregular torques are applied to the driving gear. Figure 14 shows the analysis results of torque detection error. The torque applied to the operating torque sensing system ranges from −77.7 to 63.6 mN·m; the maximum detection error is 13.56 mN·m; the maximum relative detection error is 9.60%. Additionally, the mean detection error is 0.319 mN.m, and the mean relative detection error is 0.226%.

3.2 Operation force detection evaluation

By implementing the experimental setup shown in Fig. 10b, the performance of the operating force detection method is evaluated. Because deformation of the elastic guidewire adversely affects the force equilibrium between the proposed clamping device within the slave manipulator and ATI sensor, a rigid rod is employed instead of the guidewire. In this

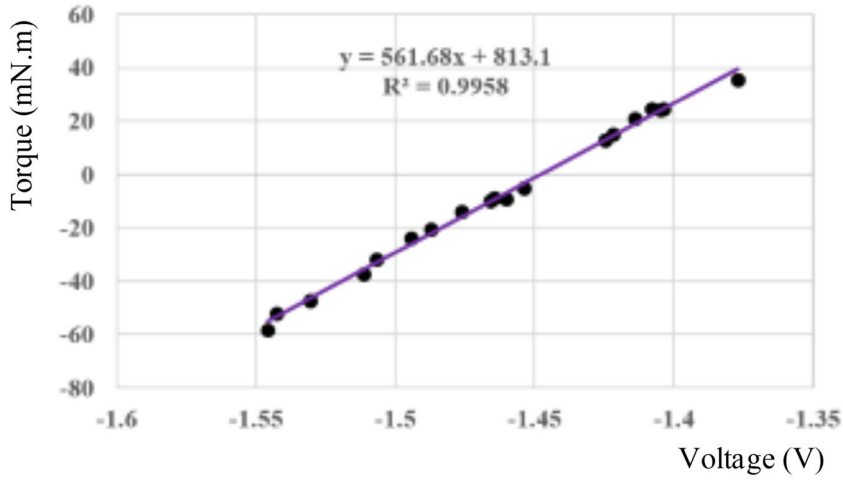

Fig. 11 Linear regression results of the proposed torque sensing sensor

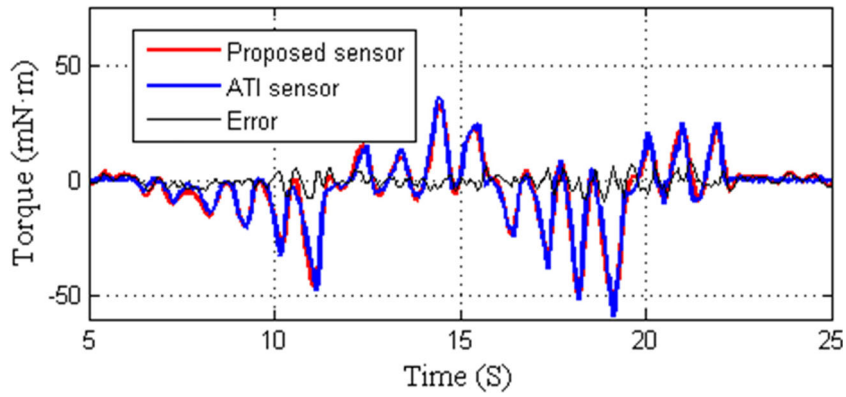

Fig. 12 Error analysis results of the proposed torque sensing device

evaluation, experiments are conducted under static and dynamic conditions. Under static conditions, the ATI sensor is repeatedly manually compressed to apply gradually increasing pressure along the axis of the rigid rod while the slave manipulator is fixed on the lead screw. Under dynamic conditions, the slave manipulator is controlled by the master controller to impact the axis of the ATI sensor via the rigid rod, while the ATI sensor is free to move along the slide way. All experiments are repeated ten times.

Figure 15 shows the results of operating force detection under static conditions. It can be seen that the force curve of the proposed sensing system and those of the ATI sensor are well matched. The maximum detection error is 0.151 N, and the maximum experimental applied force is 3.32 N. The maximum relative detection error is 4.55%; the mean detection error is 0.0345 N. In addition, the mean relative detection error is 1.04%, and the detection error variance is 0.0023 N^2.

Figure 16 shows the results of evaluating the operating force detection under dynamic conditions. It can be seen from Fig. 16 that under dynamic conditions, a sudden impact force is detected via the proposed operating force detection system and ATI system. However, although the force curve of the proposed sensing system does not match that generated via the ATI sensor under an impact force, the peak values of these two force curves are approximate equal. In the experiment, the maximum time delay between the peak values of the two force curves is about 0.19 s. Although there exists an about 0.19 s time delay, the sensing device has the capability to detect the impact force under dynamic conditions, which will be send to the master controller for haptic feedback to improve safety assurance during surgery.

3.3 Performance evaluation on EVE

To evaluate the performance of the proposed manipulator under operating conditions, the experimental setup is developed as is shown in Fig. 17. An EVE is implemented as the surgical environment, and a haptic phantom (Geomagic Touch X, produced by OR3D, Ltd) is adopted as the master controller. The phantom detects the movements of the manipulating handle and controls the slave manipulator to move the operating guidewire within the EVE. The operation experiment on the EVE is carried out by an endovascular interventional surgeon. The experimental task is designed to operate the guidewire beginning at the arcus aortae and extending to the vertebral artery through the left subclavian artery. The surgical path is shown in Fig. 18. Cooperating with axial push and pull operation, rotation operation must be performed to pass through two vessel junctions to accomplish the experimental task. The simulation operation experiment is repeated ten times.

Figure 19 shows the positions of the guidewire from p1 to p7 during the experimental procedure. From p1 to p2, the guidewire is pulled and rotated, contacting the end of the brunch of the left common carotid artery. From p2 to p3, the guidewire is pulled and rotated, contacting the end of the brunch of the left subclavian artery. From p3 to p4, the

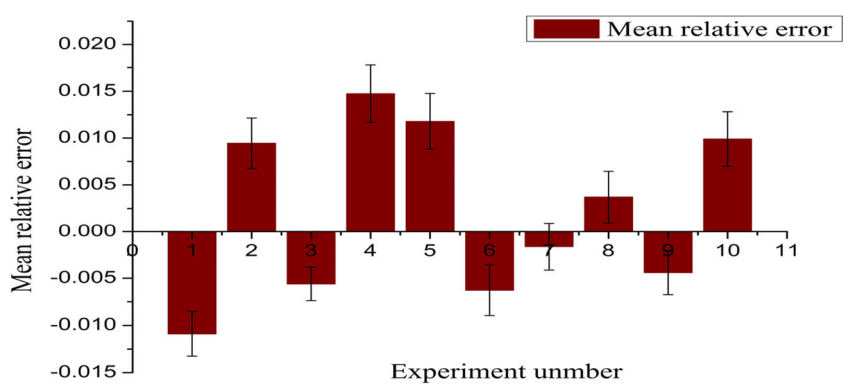

Fig. 13 Mean relative torque detection error of calibration experiments

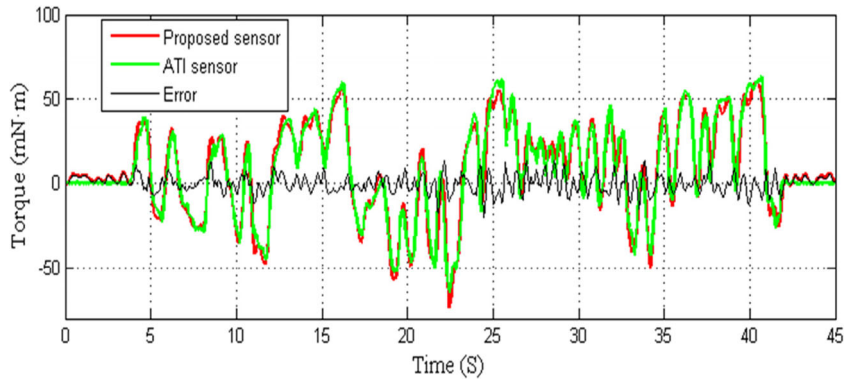

Fig. 14 Results of torque sensing device evaluation

guidewire is pushed and rotated to enable entry into the left subclavian artery. From p5 to p6, the guidewire is rotated within the left subclavian artery. From p6 to p7, the guidewire is rotated and pushed, contacting a corner of the left subclavian artery. Figure 20 shows the results of detected operation torque, comparing to rotational distance of slave manipulator. It is defined that the guidewire is rotated clockwise when angle distance of slave manipulator is reduced. Conversely, the guidewire is rotated anticlockwise when the angle distance of the slave manipulator is increased. In Fig. 20, it can also be seen that the maximum and minimum values are detected according to p1 to p7. The operating torque ranges from −19 to 24 mN·m during the experimental operating, and the average rotational speed of the guidewire is calculated as 19.3 rpm.

Figure 21 illustrates the results of the detected operation force compared to axial distance of the slave manipulator. It is defined that the guidewire is pushed when the axial distance of slave manipulator is reduced, and the guidewire is pulled when the axial distance of slave manipulator is increased. It can be seen that the operating force increases and reduces according to push and pull operation of the guidewire. The operating force ranges from −0.89 N to 0.52 N in this experimental task.

4 Discussions

The measuring range of the proposed torque sensing device is from −60 mN·m to 40 mN·m, which is about 3 times about the rotating torque variation range, which is about 30mN·m as reported by Thakur (Thakur et al. 2009b). The measuring range of the load cell adopted in this paper is −2.5 N to 2.5 N. 2.5 N is about 3 times of the maximum inserting force measured in our experiments, which is about 0.89 N. So, the maximum operation torque and force can be detected by the proposed sensing device. Figure 13 shows the mean relative errors of ten times of experiments and the standard deviation of the relative errors of every experiment. It can be seen that the maximum mean relative error is 1.45% and the standard deviation is 0.31%. It indicates that the measurement error of the proposed torque sensing device reaches the requirement in clinical surgery. The maximum detection error of typical calibration experiment is 7.9894mN·m and the maximum relative detection error is 7.91%. It should be noted that the maximum absolute detection errors are relatively large. However, because it can be seen in Figs. 12 and 14 that large detection errors correspond to dramatic changes in the operating torque, it can be deduced that the large detection error is primarily attributed to the effects of mechanical hysteresis and inertia, which could be further reduced by parameter optimization. It indicates that the proposed operation torque sensing method is promising and can be effectively implemented in robot-assisted surgical vascular intervention. In addition, the error of the proposed sensing device is also primarily caused by machining error of the crossbeam, unreliability of strain gauge installation, and electrical interference affecting the power, amplification module, and DAQ card. Therefore, error reduction could be a focus of future work.

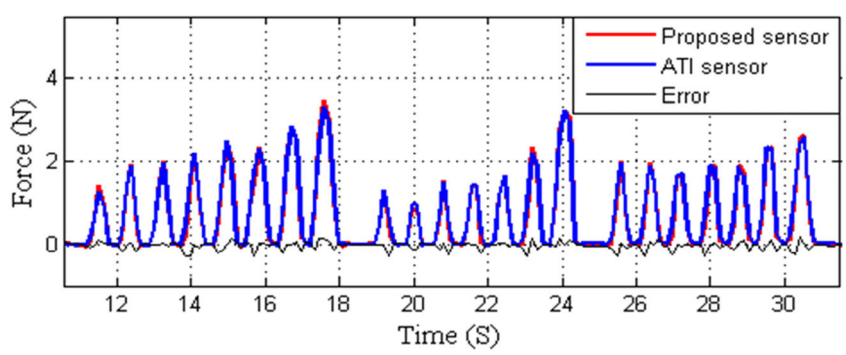

Fig. 15 Results of operating force detection performance evaluation under static conditions

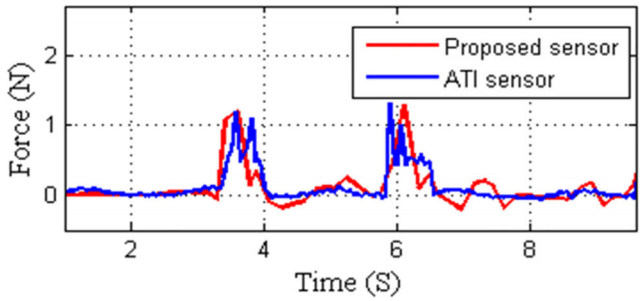

Fig. 16 Results of operating force detection performance evaluation under dynamic condition

In the static force load evaluation experiments for operating force detection, the maximum detection error is 0.151 N, and the maximum relative detection error is 4.555%. However, it can be seen from Fig. 15 that large detection errors occur at points where there are sharp changes in the force load can be observed. The main contributors to this phenomenon are considered to be the effects of mechanical hysteresis and inertia. This phenomenon is more evident in results of the dynamic force loading experiments, which are illustrated in Fig. 16. The time delay is about 0.19 s in the experiment. The primary cause of the time delay is considered to be the long force transmission distance, as is shown in Fig. 2. Moreover, the assembling error of the four slide guides also generates additional frictional effects and increased detection error. Despite these undesirable effects, the operating force detection method proposed in this study can adequately reflect the operating force conditions to provide appropriate haptic feedback to a surgeon.

The ten experimental trials employing the EVE effectively simulate the performance of the proposed robot-assisted surgery system under operating conditions. Although the operating torque and force detection accuracies cannot be quantitatively evaluated because a standard force sensor cannot be used within the EVE, the experimental results demonstrate that the fluctuating trends of the operating torque and force largely correspond to the fluctuating trends of the slave manipulator angle and axial distance, respectively. Furthermore, overall, the results show that, through the system proposed in this study, on-line acquisition of the operating force information can be realized for robot-assisted surgical vascular intervention.

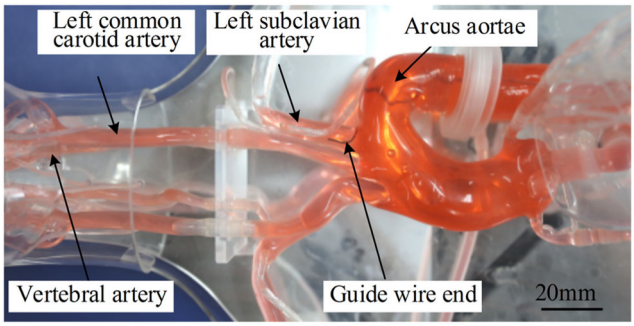

(a) Top view of the EVE

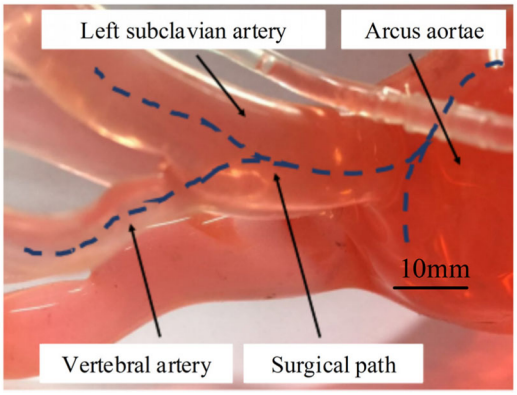

(b) Diagram of surgical path

Fig. 18 Vascular access of simulated operation experiments

5 Conclusion

In this paper, a novel slave manipulator of the robot endovascular interventional surgery system is proposed for on-line acquisition of operation force information during robot-assisted surgical vascular intervention.

The designed torque and force detection device enables on-line acquisition of small-scale operating torque and force of the guidewire under low rotational speed. Moreover, the experimental results indicate that the proposed operating torque sensing method has the potential to significantly increase the efficacy of robot-assisted surgical vascular intervention.

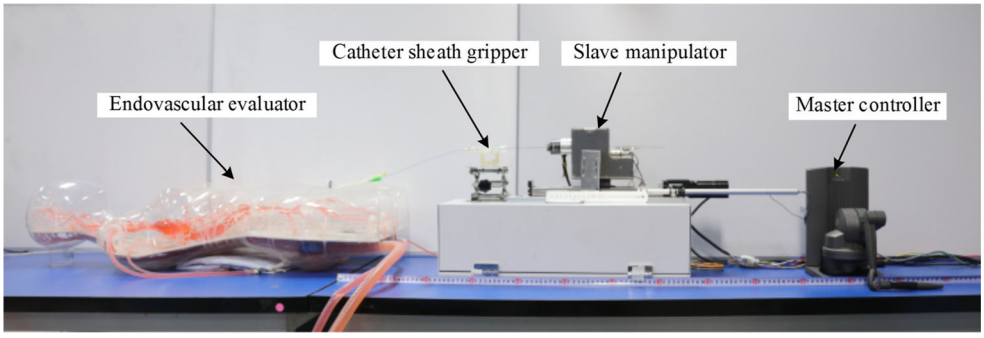

Fig. 17 Experimental setup for simulated operation on the EVE

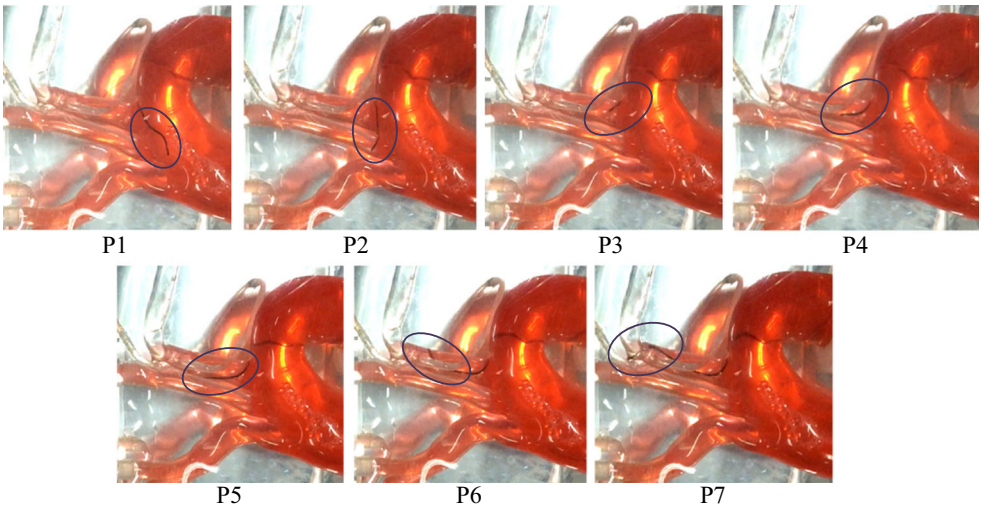

Fig. 19 Experimental operation results: respective guidewire positions according to p1 to p7

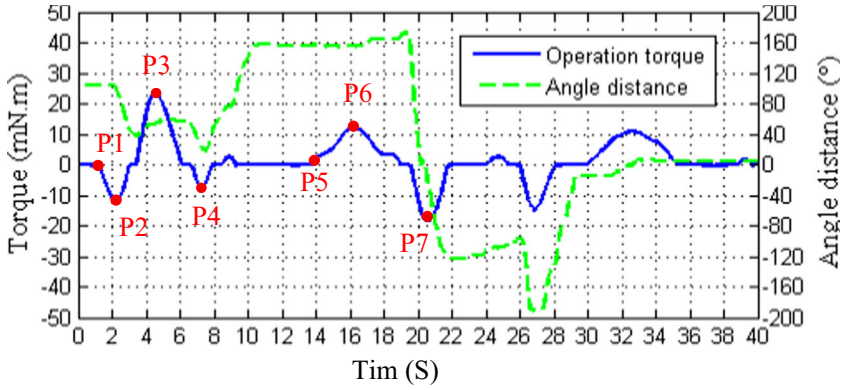

Fig. 20 Results of detected operating torque compared to angle distance of slave manipulator

Additionally, in the evaluation experiments on the EVE, the fact that the desired tasks were successfully accomplished with relatively minimal difficulty confirmed that the proposed slave manipulator can be practically applied. Furthermore, it has been demonstrated that this system enables enhanced perception of the operating conditions from the perspective of the slave manipulator.

In future work, the machine accuracy of the crossbeam and strain gauge installation process could be improved to reduce the operating torque detection error. Additionally, the electrical interference affecting the operating torque sensing system should be eliminated. Furthermore, mechanical structure of operating force detection device should be optimized to reduce the detection error. Lastly, future work should focus on transmitting the operating force information to the master system to enable accurate haptic feedback to the surgeon for improved surgical safety.

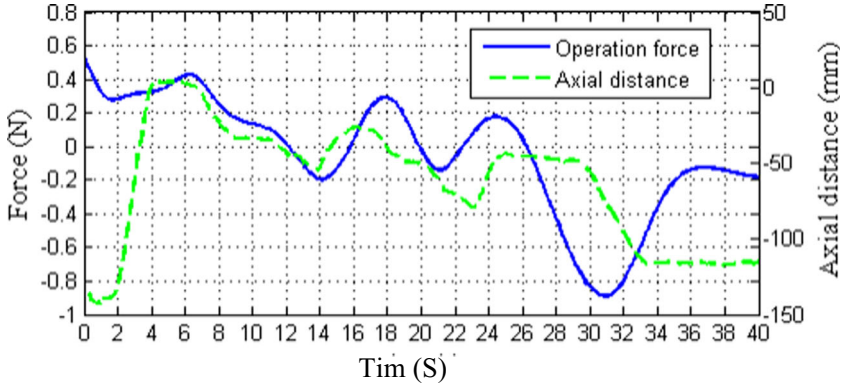

Fig. 21 Results of detected operating force compared to axial distance of slave manipulator

Acknowledgements This research is partly supported by the National High Tech. Research and Development Program of China (No.2015AA043202), and National Natural Science Foundation of China (61375094, 61503028).

References

J. Back, R. Karim, Y. Noh, K. Rhod, K. Althoefer, H. Liu, *Tension sensing for a linear actuated catheter robot. Intelligent robotics and applications. ICIRA 2015. Lecture notes in computer science, 9245* (Springer, Cham, 2015), pp. 472–482

L. Cercenelli, B. Bortolani, E. Marcelli, CathROB: A highly compact and versatile remote catheter navigation system. Applied Bionics and Biomechanics **2017**(8), 1–13 (2017)

J. Dankelman, J.J. van den Dobbelsteen, P. Breedveld, in *Proceedings of 2011 International Conference on Instrumentation Control and Automation*. Current technology on minimally invasive surgery and interventional techniques (IEEE Press, Bandung, 2011), pp. 12–15

T. Datino, A. Arenal, P.M. Ruiz-Hernández, M. Pelliza, J. Hernández-Hernández, E. González-Torrecilla, F. Atienza, P. Ávila, F. Fernández-Avilés, Arrhythmia ablation using the amigo robotic remote catheter system versus manual ablation: One year follow-up results. Int. J. Cardiol. **202**, 877–878 (2015)

R.A. Dello, G. Fassini, S. Conti, M. Casella, A.D. Monaco, E. Russo, S. Riva, M. Moltrasio, F. Tundo, G.D. Martino, G. Gallinghouse, L.D. Biase, A. Natale, C. Tondo, Analysis of catheter contact force during atrial fibrillation ablation using the robotic navigation system: Results from a randomized study. J. Interv. Card. Electrophysiol. **46**(2), 97–103 (2016)

D. Filgueiras-Rama, A. Estrada, J. Shachar, S. Castrejón, D. Doiny, M. Ortega, E. Gang, J.L. Merino, Remote magnetic navigation for accurate, real-time catheter positioning and ablation in cardiac electrophysiology procedures. Journal of Visualized Experiments Jove. **74**(74), e3658–e3658 (2013)

D. Gelman, A.C. Skanes, M.A. Tavallaei, M. Drangova, Design and evaluation of a catheter contact-force controller for cardiac ablation therapy. IEEE Trans. Biomed. Eng. **63**(11), 2301–2307 (2016)

J. Guo, G. Shuxiang, Design and characteristics evaluation of a novel VR-based robot-assisted catheterization training system with force feedback for vascular interventional surgery. Microsyst. Technol. **23**, 1–10 (2016)

J. Guo, S. Guo, N. Xiao, X. Ma, S. Yoshida, T. Tamiya, M. Kawanishi, A novel robotic catheter system with force and visual feedback for vascular interventional surgery. International Journal of Mechatronics and Automation. **2**(1), 15–24 (2012)

J. Guo, S. Guo, L. Shao, P. Wang, Q. Gao, Design and performance evaluation of a novel robotic catheter system for vascular interventional surgery. Microsystem Technology. **22**(9), 1–10 (2015)

J. Guo, S. Guo, Y. Yu, Design and characteristics evaluation of a novel teleoperated robotic catheterization system with force feedback for vascular interventional surgery. Biomed. Microdevices **18**(5), 76 (2016)

F. Kiemeneij, M.S. Patterson, G. Amoroso, G. Laarman, T. Slagboom, Use of the Stereotaxis Niobe® magnetic navigation system for percutaneous coronary intervention: Results from 350 consecutive patients. Journal of Catheterization and Cardiovascular Interventions. **71**(4), 510–516 (2008)

X. Liu, G. Xu, R. Zhang, *Endovascular management for stroke* (People's medical publishing house, Beijing, 2006), pp. 134–136

Y. Song, S. Guo, X. Yin, L. Zhang, Y. Wang, H. Hirata, H. Ishihara, Design and performance evaluation of a haptic interface based on MR fluids for endovascular tele-surgery. Microsystem Technologies, 1–10 (2017)

Y. Thakur, J.S. Bax, D.W. Holdsworth, M. Drangova, Design and performance evaluation of a remote catheter navigation system. IEEE Trans. Biomed. Eng. **56**(7), 1901–1908 (2009a)

Y. Thakur, D.W. Holdsworth, M. Drangova, Characterization of catheter dynamics during percutaneous transluminal catheter procedures. IEEE Trans. Biomed. Eng. **56**(8), 2140–2143 (2009b)

V. Vitiello, K.W. Kwok, G. Yang, Introduction to robot-assisted minimally invasive surgery (MIS). Medical Robotics: Minimally Invasive Surgery **2**(1–4), 1–40 (2012)

Y. Wang, S. Guo, B. Gao, Vascular Elastcity determined mass-spring model for virtual reality simulators. International Journal of Mechatronics and Automation. **5**(1), 1–10 (2015)

Y. Wang, S. Guo, T. Tamiya, H. Hirata, H. Ishihara, X. Yin, A virtual-reality simulator and force sensation combined catheter operation training system and its preliminary evaluation. International Journal of Medical Robotics and Computer Assisted Surgery. **13**, e1769 (2016)

N. Xiao, J. Guo, S. Guo, T. Tamiya, A robotic catheter system with real-time force feedback and monitor. Australasian Physical & Engineering Sciences in Medicine **35**(3), 283–289 (2012)

X. Yin, S. Guo, H. Hirata, H. Ishihara, Design and experimental evaluation of a Teleoperated haptic robot assisted catheter operating system. J. Intell. Mater. Syst. Struct. **27**(1), 3–16 (2014)

X. Yin, S. Guo, N. Xiao, T. Tamiya, H. Hirata, H. Ishihara, Safety operation consciousness realization of a MR fluids-based novel haptic Interface for teleoperated catheter minimally invasive Neuro surgery. IEEE/ASME Transactions on Mechatronics. **21**(2), 1043–1054 (2015)

L. Zhang, S. Guo, H. Yu, Y. Song, Performance evaluation of a strain-gauge force sensor for a haptic robot-assisted catheter operating system. Microsyst. Technol. **5**, 1–10 (2017)